PHYSICAL REVIEW A VOLUME 20, NUMBER 3 SEPTEMBER 1979

Role of excited electronic states in the interactions of fast (MeV) molecular ions with solids and gases

E. P. Kanter, P. J. Cooney,* D. S. Gemmell, K.-O. Groeneveld,† W. J. Pietsch,‡ A. J. Ratkowski,§ Z. Vager,‖ and B. J. Zabransky

Physics Division, Argonne National Laboratory, Argonne, Illinois 60439

(Received 23 February 1979)

The authors report measurements of the joint distributions in energy and angle for fragments arising from the dissociation of 1.2-MeV H_2^+ and 3.0-MeV HeH^+ in thin carbon foils and in a variety of gases at several pressures. From the foil measurements the distribution of initial internuclear separations in the incident projectiles is derived. These distributions are then used in conjunction with the results for gas targets to determine the role of excited electronic states of the projectile in collisionally induced dissociation. Finally, it is shown how these states also play a vital role in some other phenomena that occur in the interactions of fast molecular ions with foils.

I. INTRODUCTION

The collision-induced dissociation of molecular ions has been previously studied, mostly with gaseous targets and with ion-beam energies in the keV range (for a recent review, see Ref. 1). In this field, the term "high energy" has come to mean beam energies of a few tens of a keV. There are, however, some definite advantages in extending such studies to ion velocities of an order of magnitude higher, i.e., to beam energies in the MeV range. For light projectiles at these energies, the time for a typical collision with a target atom is short enough ($\sim 10^{-17}$ s) [compared with the times for molecular vibration ($\sim 10^{-14}$ s) and rotation ($\sim 10^{-12}$ s)] that during the collision the nuclei of an incident molecular ion may be considered to be stationary in the projectile frame. Furthermore, the collision time is short compared with the characteristic times for the possible dissociation modes—these times extend down to about a femtosecond (10^{-15} s) for those dissociations that arise from "Coulomb explosions" (the rapid flying apart of the nuclear constituents of a molecular projectile when all or most of its electrons are stripped away in a collision). Thus for high projectile velocities ($v \gg v_0 = e^2/\hbar$) it can be expected that, to an excellent approximation, collision-induced dissociation may be treated as a two-step process. First, there occurs a rapid collision with a target atom during which the projectile's nuclei do not move in their c.m. (center-of-mass) frame. Because of their low mass the electrons associated with the projectile reconfigure themselves in a time comparable with the collision time (this process includes the possibility of removal by ionization of some or all of the electrons). There then follows, on a much longer time scale, a dissociation of the resultant excited molecular state into two or more atomic or molecular fragments. At these projectile velocities, excitation mechanisms other than electronic excitation (e.g., rotational/vibrational excitation due to a large momentum transfer to one of the projectile nuclei) can be expected to play relatively minor roles.[2]

There are several other approximations that acquire improved validity at MeV bombarding energies. For example, energy losses (typically a few eV) due to inelastic collision processes may be neglected. The deflection of the projectile's c.m. during the collision may be neglected. A Born-approximation treatment of the collision is expected to be more fully justified at high projectile velocities. (For detailed discussions concerning these and other approximations, see Refs. 3 and 4, and references contained therein.)

The main difficulty in studying collision-induced dissociation at MeV energies is the technical one of obtaining adequate angular resolution. The fragments emerging from a collision are contained within narrow cones centered on the beam direction. The angular widths of these cones are approximately inversely proportional to the projectile velocity. At MeV energies the width of such a cone is typically a few milliradians (mrad), and thus an overall angular resolution of $\sim 10^{-4}$ radians is usually required. In the work described in this article, an angular resolution of 3×10^{-4} radians was employed. A corresponding resolution in measuring the momenta of the collision fragments is also needed, but in practice is not so difficult to achieve. The relative momentum resolution used in the work described here was also 3×10^{-4} (a relative energy resolution of 6×10^{-4}).

A significant advantage in using MeV bombarding energies lies in the fact that the measurements can be readily extended to include thin solid targets. At keV energies, use of even the thinnest and

lightest foils (e.g., ~100-Å-thick carbon) introduces a serious worsening in resolution because of energy-loss straggling and multiple scattering. Of these, the effects of multiple scattering are the most crippling. However, as the projectile velocity V_0 is raised, there is a decline not only in the absolute values of the multiple-scattering angles (which vary as V_0^{-2}), but also in the values relative to the cone angles (which vary as V_0^{-1}). As an example, the full width at half-maximum (FWHM) of the multiple-scattering distribution for 1-MeV protons traversing a 100-Å-thick carbon foil is 7×10^{-4} radians, while the average energy loss of these protons is ~500 eV and the straggling width is only a few tens of an eV.

For light projectiles (H_2^+, HeH^+, He_2^+, etc.) incident at these energies upon a foil, the electrons that bind the projectile are almost always totally stripped off within the first few angstrom of penetration into the solid target. This is a consequence of the large cross sections (~10^{-16} cm^2) for electron loss[5] and of the fact that close collisions with target electrons cannot be avoided in a solid. There then follows a Coulomb explosion in which the bare (or nearly bare) nuclei of the projectile fly apart by virtue of their mutual Coulomb repulsion. The characteristic time for this explosion is typically ~10^{-15} s, which is on the same order as the dwell time of the projectile in the foil, if the latter is about 100 Å thick. It is therefore to be expected that much of the Coulomb explosion takes place inside the foil and that it then runs to completion in the vacuum downstream after the fragments emerge from the traget. Inside the target the individual fragment trajectories are also influenced by multiple scattering and by effects due to the electron polarization "wakes" induced behind each of the fragments traversing the foil. These wake effects have been shown[6,7] to give rise to easily observable modifications to the pattern of trajectories measured downstream from the target.

For dilute gaseous targets, on the other hand, it is to be expected that most collisions will be much less violent than those in foil targets. On the average there will be fewer electrons removed from the projectile and, correspondingly, a greater probability for dissociation into less highly charged fragments. There should be no observable effects due to wakes or to multiple scattering. These general expectations have in fact been confirmed in those few measurements reported thus far[8,9] comparing results for gas and foil targets and with MeV projectiles [12-MeV OH^- (Refs. 8 and 9), and 3.7-MeV $^3HeH^+$ and 2.8-MeV OH^+ (Ref. 8)].

In this article we report on detailed measurements of the joint distributions in energy and angle for various fragments arising from the dissociation of 1.2-MeV H_2^+ and 3.0-MeV HeH^+ in thin carbon foils and in a variety of gases at several pressures. Section II gives a description of the experimental arrangements used in both the solid- and gas-target experiments, the results of which are presented in Sec. III. Section IV describes the procedures we used in extracting from the foil measurements the distribution of initial separations in the incident projectiles. These distributions are then used to analyze the gas data. In a discussion of the "reflection method" we show how the role of excited electronic states in the dissociation process can be determined. Finally, in Sec. V, we describe how consideration of these states is important in understanding some hitherto unexplained phenomena that are observed in the interactions of fast molecular-ion beams with matter.

II. EXPERIMENTAL ARRANGEMENT

The apparatus used in these measurements is essentially the same as that used in recent measurements[8,10-12] on the foil-induced dissociation of various molecular-ion beams produced by Argonne's 4-MV Dynamitron accelerator.

A. Foil targets

Figure 1 shows the arrangement used with foil targets. Magnetically analyzed molecular-ion beams were collimated to have a maximum angular divergence of ±0.09 mrad at the target position. The primary ion source used was a duoplasmatron fed with a mixture of 90% He and 10% H_2. Some measurements also utilized an rf source. The targets were mounted on a movable rack holding seven self-supporting carbon foils about 100 Å thick (the actual individual foil thicknesses were determined by α-particle energy-loss techniques). To prevent the buildup of carbon on the foils during irradiation they were heated continuously at 150 °C and surrounded by a liquid-nitrogen-cooled copper cold shield containing small holes for the entrance of the beam and for the exit of particles to be detected. The base vacuum in the target chamber was 10^{-7} Torr.

A set of "predeflector" plates permitted electrostatic deflection of the beam incident on the target. Similarly, a set of "postdeflectors" was used to deflect charged particles emerging from the target. These deflectors were calibrated by measuring the deflection of the beam spot several meters downstream (with no target) for various deflector voltages. The pre- and postdeflectors were used in combination to avoid detecting particles that arose from spurious incident beams (e.g., fragments arising from dissociation of the pri-

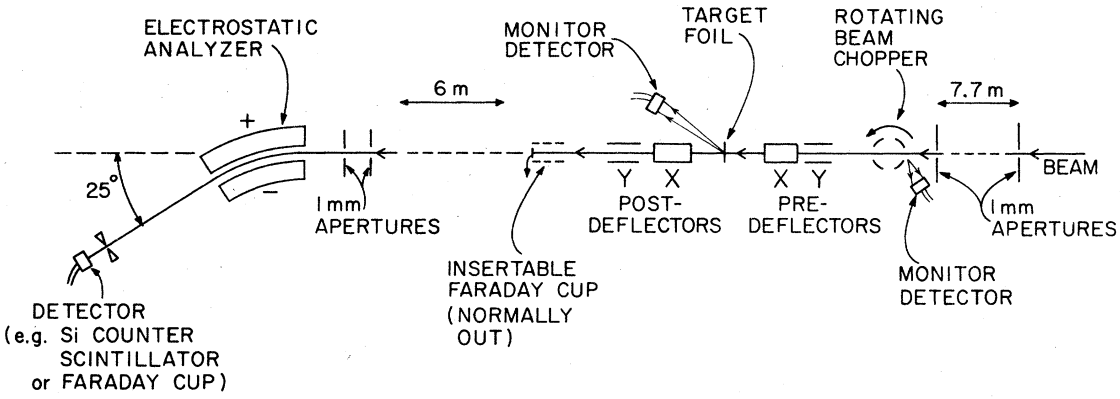

FIG. 1. Schematic diagram of the experimental arrangement used for solid targets.

mary beam along the long flight path between the beam collimators).

A 25° electrostatic analyzer having a relative energy resolution of 6×10^{-4} (FWHM) was located several meters downstream from the target. The analyzer could hold up to 40 kV across its 2.5-mm gap. This permitted it to be used for particles with energies up to 4.5 MeV per unit charge. An aperture placed ahead of the analyzer accepted a 1-mm-diameter group of trajectories originating at the target position. To permit certain classes of measurements on neutral fragments the entrance axis of the analyzer was offset horizontally by 2 mrad from the direction defined by the collimators for the incident beam. [Neutrals were detected by applying a high field across the horizontal, or "X", postdeflectors to remove charged fragments and then by stripping the neutrals at the analyzer entrance aperture using a thin (~100-Å) carbon foil insertable for that purpose.] A silicon surface-barrier detector counted particles emerging from the exit slit of the analyzer. Count rates up to a maximum of 20 000/s were employed. The energy-resolving capability of the silicon detector was useful in ensuring that the desired fragments were indeed the ones being counted.

To avoid the influence of the earth's and other stray magnetic fields on the particle trajectories, it was necessary to shield magnetically (with mu metal) the several-meters-long flight paths traversed by the incident beam and by the exciting fragments.

Distributions in energy and angle were made for particles emerging from the target by varying the voltages on the horizontal predeflectors and/or postdeflectors in conjunction with that on the electrostatic analyzer. (The vertical, or "Y", deflectors were normally used only for "trimming" purposes.) With the arrangement of collimating apertures indicated in Fig. 1, the overall angular resolution was 0.3 mrad (FWHM), and the beam-spot size at the target was 1 mm. The deflector and analyzer voltages were set and read out by an on-line PDP-11/45 computer system that controlled modules in a CAMAC crate via a serial data highway. In addition to its other monitoring and control functions, the computer also positioned (horizontally) the target rack with an accuracy of ±0.1 mm. This permitted the automatic changing of targets and the adjustment of the target position needed in conjunction with use of the X predeflector to maintain the position of the beam spot on the target.

Monitoring of the incident-beam current was achieved with a rotating chopper which intercepted the beam about 50% of the time. Particles scattered from the chopper were counted in a silicon surface-barrier detector. The absolute efficiency of this device could be determined when necessary by calibration, using an insertable Faraday cup and a beam-current integrator. Beam currents of about 1 nA were typical during these experiments.

The target thickness (and also the composition of both beam and target) was monitored with another silicon detector counting particles scattered or knocked out of the target at 45° to the beam direction. It was usually found that the amount of carbon in a virgin carbon-foil target would decline by about 20% over the first few minutes of irradiation with the beam and would then stay constant for a week or more.

B. Gas targets

The arrangement used for measurements with gas targets was similar to that described above except that the foil rack and cold shield were replaced by a differentially pumped 10-cm-long gas cell, the design of which is indicated schematically in Fig. 2. The axis of this cell was offset horizontally by 10 mrad, relative to the direction de-

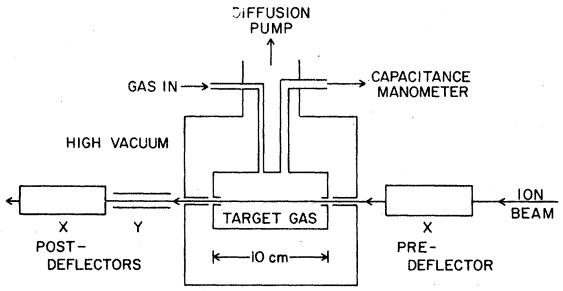

FIG. 2. Schematic diagram of the differentially pumped gas target.

fined by the beam collimators. The incident beam was therefore always given a corresponding X predeflection to bring it into the cell. The entrance aperture to the cell was 2 mm in diameter, and the exit aperture was a horizontal slit 2 mm high by 6 mm wide. The pressure in the cell, which was measured with a capacitance manometer, could be varied from the base pressure of the scattering chamber ($\sim 10^{-7}$ Torr) up to ~ 500 mTorr. At a cell pressure of 500 mTorr, the pressure in the scattering chamber rose to $\sim 10^{-5}$ Torr.

III. EXPERIMENTAL RESULTS

A. Foil targets

Joint energy-angle distributions for protons arising from the foil-induced dissociation of MeV beams of H_2^+ and HeH^+ have been the topic of several recent investigations (see Refs. 6, 8, and 12–15 for H_2^+; Refs. 6–8, 11, 12, and 14 for HeH^+). In this article we therefore restrict ourselves to showing just one such distribution for each molecular ion (see Figs. 3 and 4). The most obvious feature to be noted in these distributions is that they are "ring patterns," as is to be expected on the basis of a simple Coulomb explosion picture of the dissociation process. The diameter of the ring is determined primarily by the bond length in the projectile. The width of the "rim" of the ring reflects the range of internuclear distances present in the projectiles as they enter the target. Wake effects manifest themselves through slight distortions of the ring. The ring is thereby stretched along the energy axis and contracted along the angle axis. The stretching along the energy axis is actually the result of two effects—a contraction of the energy shift on the high-energy side coupled with a (larger) stretching of the energy shift on the low-energy side. This asymmetry along the energy axis is further accentuated by the pronounced increase in proton intensity on the low-energy side of the ring as compared with the smaller increase on the high-energy side. For more detailed discussions of all of these effects the reader is referred to the other work noted above. In particular, the influence of wake effects

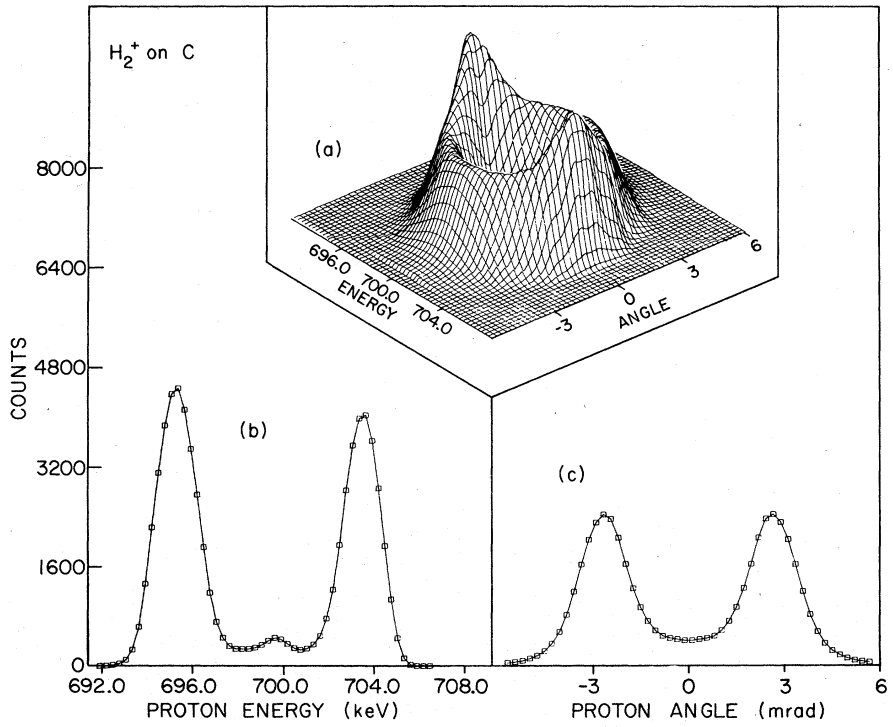

FIG. 3. (a) Joint energy-angle distribution for protons arising from the dissociation of 1.4-MeV H_2^+ in an 88-Å-thick carbon foil. (b) The corresponding energy spectrum of those protons emerging from the target foil in the beam direction. (c) The corresponding angular distribution of those protons emerging from the target with an energy halfway between the two peaks in (b). A complete joint distribution such as (a) is termed a "ring pattern" while a complementary pair of spectra such as (b) and (c) is termed a "cross."

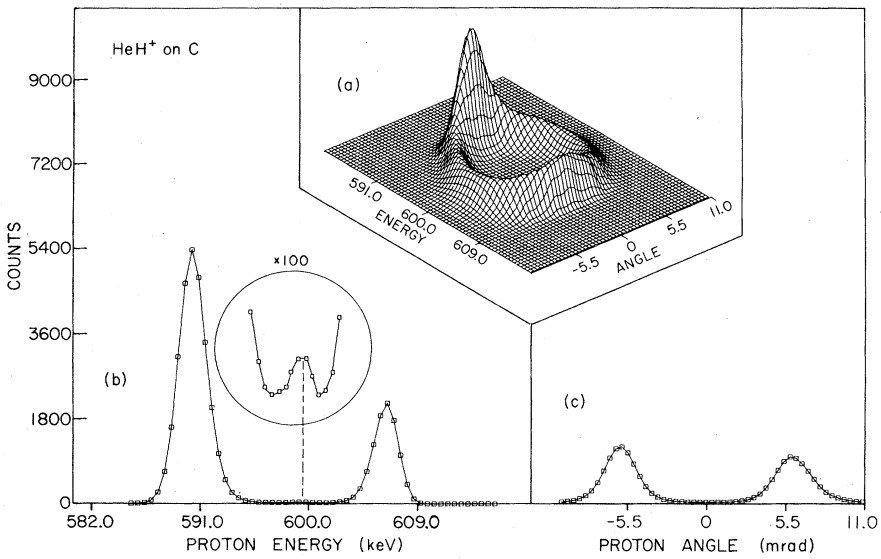

FIG. 4. (a) Ring pattern and (b), (c) cross for protons from the dissociation of 3.0-MeV HeH^+ in a 195-Å-thick carbon foil.

is treated more fully in Ref. 7.

Most of our data on the fragments arising from molecular-ion dissociation take the form of measurements either of a complete ring pattern or of a "cross" [i.e., an energy distribution for zero angle shift together with an angle distribution for zero energy shift (allowing for the usually trivially small energy loss due to the stopping power of the target)]. A cross thus represents the two distributions obtained by cuts along the energy and angle axes of the ring pattern. In Figs. 3 and 4 we show both rings and crosses.

In the crosses of Figs. 3 and 4 one notes (on an expanded scale) the presence of a "central peak." This narrow peak which has been observed previously[8,11,16] in the case of foil-induced dissociation corresponds to protons emerging from the target with a velocity essentially unshifted from that of the incident beam. The width of the peak is slightly larger than the experimental resolution in energy and angle. We return in more detail to the origin and significance of this peak in following sections.

B. Gas targets

To the best of our knowledge there have been no previously reported measurements of the joint energy and angle distributions for fragments from fast (MeV) molecular ions dissociating in a gas. For this reason we give more emphasis in this article to results obtained for gas targets than to those for foil targets.

We have measured crosses and (less frequently) ring patterns for 1.2-MeV H_2^+ and 3.0-MeV HeH^+ projectiles dissociating in a variety of target gases (H_2, He, N_2, Ar, CO_2, Xe, and SF_6) for pressures in the range 1–500 mTorr.

Our first observation was that the shapes of the distributions when measured at low target-gas pressures (single collision regime) did not display any marked dependence on the species of the target gas. [We had anticipated that, as one progressed to targets containing large numbers of electrons (e.g., Xe and SF_6), some effects characteristic of those for solid targets might be encountered.]

Next we note that for crosses measured at low target pressures, the shapes of the energy and angle distributions are almost identical. Furthermore, they are symmetric—there is no evidence of any wake effect. As the target-gas pressure is raised (see Fig. 5), the shapes of the distributions begin to differ. At the highest pressures the angle distributions lose their fine structure, while the energy distributions retain theirs. This "washing out" of structure in the angle dimension is not simply due to the increase in multiple scattering [e.g., for the case of 163 mTorr of Ar shown in Fig. 5, the multiple scattering of 600-keV protons is calculated to contribute a "smearing" of ~1.6 mrad (FWHM)]. Rather, it is probably an instrumental effect caused by interactions with gas that leaks into the deflector plate gaps at these high pressures. The energy spectra are not affected by this.

The distributions are dominated by a central peak, whose width when measured at low target pressures is about 1–2 times the experimental resolution. The width is slightly less for light target gases (e.g., He) and slightly more for heavy target gases (e.g., Ar).

At a given target-gas pressure, a measure of the yield for one dissociation fragment can be obtained from a distribution in either energy or angle

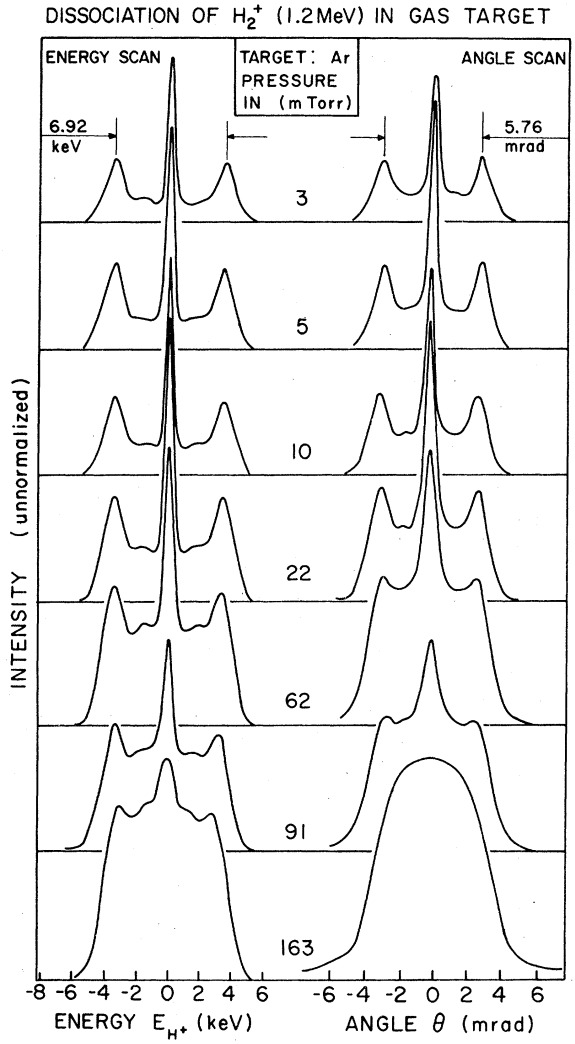

FIG. 5. Crosses for protons from the dissociation of 1.2-MeV H_2^+ in Ar at various pressures.

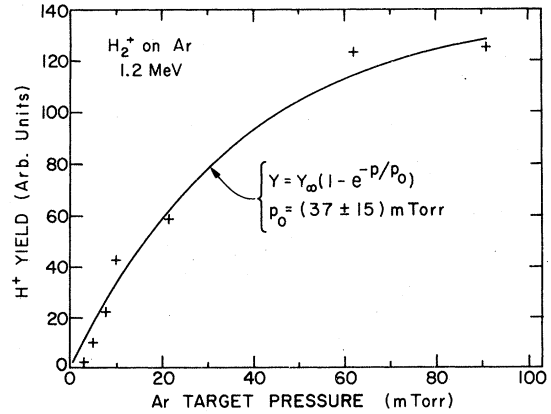

FIG. 6. Pressure dependence of the yield of protons from the dissociation of 1.2-MeV H_2^+ in Ar. The solid curve is a least-squares fit to the data points.

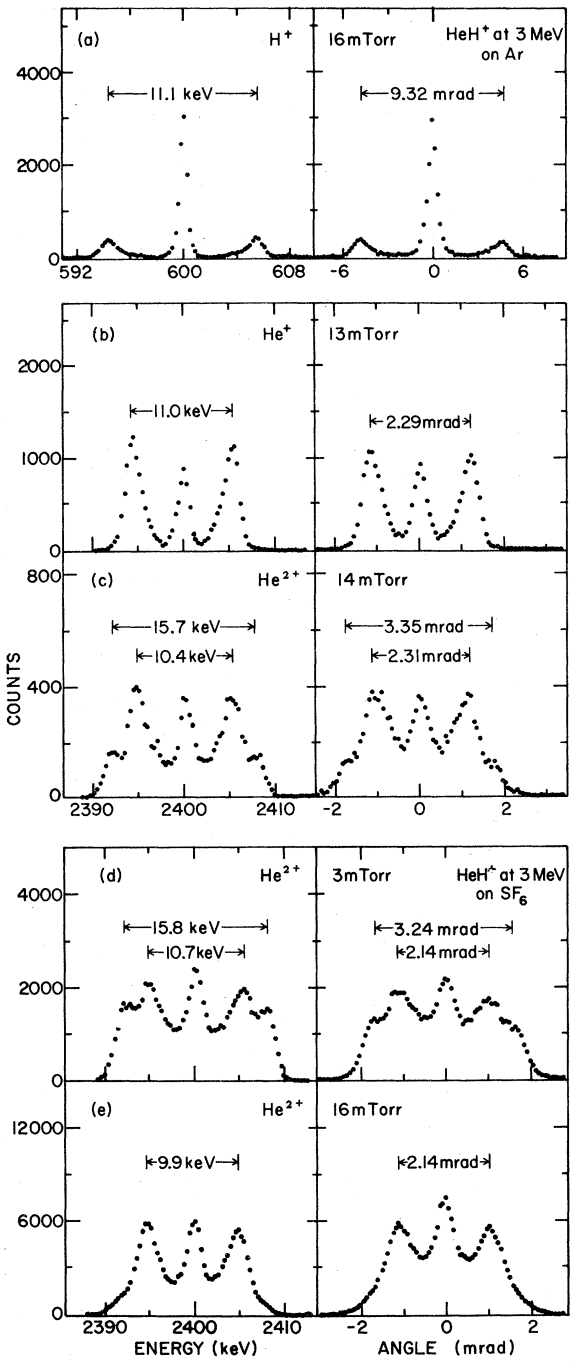

FIG. 7. Crosses for H^+, He^+, and He^{2+} ions from the dissociation of 3.0-MeV HeH^+ in Ar and SF_6.

by evaluating

$$Y = \sum_k (k - \bar{k})^2 N_k , \tag{1}$$

where N_k is the kth element of the distribution and $\bar{k}$ is the mean value of k. The reasons for this

choice of an expression for the yield are elucidated in Sec. IV C. Yields evaluated from both energy and angle spectra agreed to $<0.5\%$.

Figure 6 shows some results for protons from 1.2-MeV H_2^+ dissociating in argon. The solid curve in Fig. 6 shows a fit to the data points with a function of the form

$$Y(p) = Y_\infty[1 - \exp(-p/p_0)], \tag{2}$$

where p is the gas pressure. From the pressure p_0 thus obtained, one can evaluate the mean free path and a corresponding total dissociation cross section. For the data shown in Fig. 6, $p_0 = 37 \pm 15$ mTorr, and the dissociation cross section is $\sigma_D = (0.8 \pm 0.3) \times 10^{-16}$ cm^2.

For the case of 3.0-MeV HeH^+ we have measured distributions for H^+, He^+ and He^{2+} fragments. Figures 7(a)–7(c) show crosses for these fragments emerging from Ar at ~15 mTorr. Again the distributions exhibit pronounced central peaks. In the H^+ distribution, the peaks on either side of the central peak result from dissociation leading to $H^+ + He^+$. The small number of counts seen outside of these peaks are due to dissociation leading to $H^+ + He^{2+}$. Clearly the second of these two dissociation modes is much less probable than the first. Table I gives the peak separations expected for a simple, pure Coulomb explosion of point charges; such a model is unrealistically simple, but is a guide to classifying the peaks observed. The He^+ distributions show a central peak and just one set of side peaks. The side peaks correspond closely to those expected for dissociations leading to $H^+ + He^+$. Somewhat surprisingly, the He^{2+} distributions exhibit the same three peaks as the He^+ distribution (with the same separations) together with a rather weak contribution from another pair of peaks corresponding to dissociations giving $H^+ + He^{2+}$. The relative intensity of this latter pair of peaks decreases as the target-gas pressure increases. For example, at low pressures in SF_6 [see Fig. 7(d)] the five individual peaks can be seen quite clearly, while only the three inner peaks are visible at a higher pressure [see Fig. 7(e)]. Thus all of the evidence points to the $H^+ + He^+$ mode as being much more probable than the direct $H^+ + He^{2+}$ dissociation mode. The majority of the detected He^{2+} ions evidently come from He^+ ions that later lose an electron in another gas collision. Figure 8 shows data on the pressure dependence of the yields for the fragments H^+, He^+, and He^{2+}, along with fits to the data suggested by this simple model for H^+, He^+, and He^{2+} production.

From data such as those given in Figs. 6 and 8, we can extract dissociation cross sections. The results for Ar are given in Table II, along with

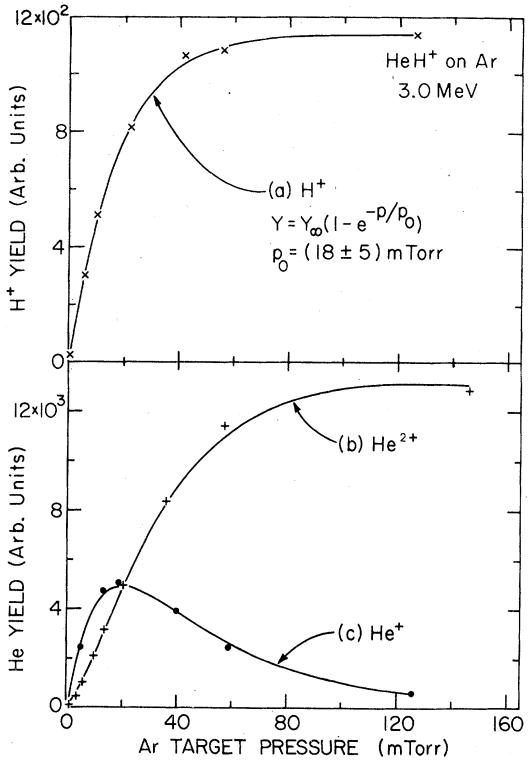

FIG. 8. Pressure dependence of the yield of H^+, He^+, and He^{2+} from the dissociation of 3.0-MeV HeH^+ in Ar. The curves are least-squares fits to the data points.

TABLE I. Classical estimates of the "ring" diameters ΔE (keV) and $\Delta\theta$ (mrad), when an energy $Z_1Z_2e^2/r_0$ is liberated in the c.m. system of an incident 3.0-MeV HeH^+ ion having $r_0 = 0.77$ Å.

Outgoing fragment	Z_1Z_2 =	ΔE (keV) 1	ΔE (keV) 2	$\Delta\theta$ (mrad) 1	$\Delta\theta$ (mrad) 2
H		12	17	10	14
He		12	17	2.5	3.5

TABLE II. Estimated cross sections (Å^2/molecule) for the dissociation of H_2^+ and HeH^+ incident on various gas targets at 600 keV/amu. Overall experimental uncertainties are typically ±40%.

Target	$H_2^+ \rightarrow H^+$	$HeH^+ \rightarrow H^+$
He	0.16	0.5
Ar	0.8	1.8
Xe	1.7	•••
H_2	0.19	•••
N_2	1.6	1.9
CO_2	1.4	•••
SF_6	1.4	•••

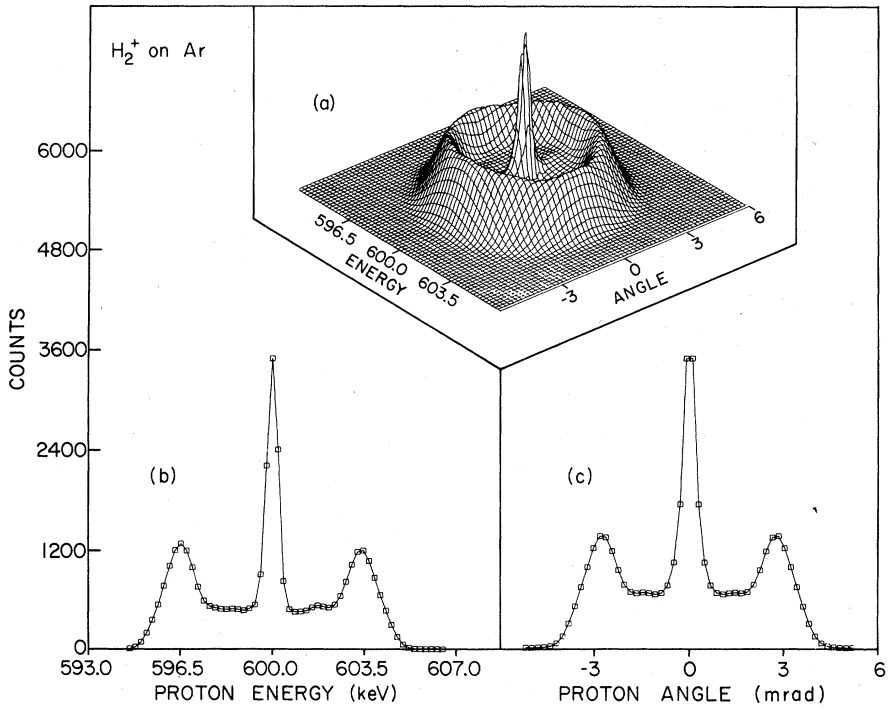

FIG. 9. (a) Ring pattern and (b), (c) cross for protons from the dissociation of 1.2-MeV H_2^+ in Ar at 7.8-mTorr pressure.

estimates of the dissociation cross sections in a number of other gases. The latter estimates are based on measurements of the relative yields from each gas and on the assumption that the branching ratios for the various dissociation modes are independent of the target-gas species. As the aim here was merely to define that range of pressures for each gas which would assure single-collision conditions, no attempt was made to measure these dissociaton cross sections to a greater accuracy. The values given in Table II are consistent with cross sections determined by previous workers[17,18] and are roughly on the order of atomic geometric cross sections, as one might expect.[2]

Curves such as those of Figs. 6 and 8 clearly indicate a transition from a low-pressure regime where single collisions dominate to a regime where multiple collisions occur. Since single collisions are the fundamental phenomena of physical interest, we restrict ourselves in the remainder of this

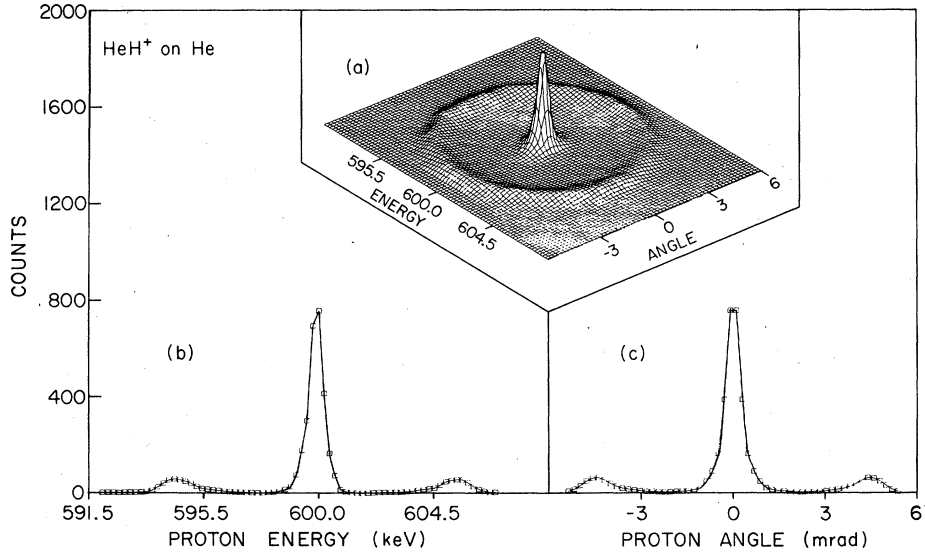

FIG. 10. (a) Ring pattern and (b), (c) cross for protons from the dissociation of 3.0-MeV HeH^+ in He at 9.5 mTorr pressure.

article to discussion of the low-pressure (single-collision) regime.

Figures 9 and 10 show complete ring patterns for protons from 1.2-MeV H_2^+ and 3.0-MeV HeH^+ dissociating in argon and helium, respectively. One sees very clearly the dominant central peak and the overall symmetry of the distributions. It is worth remarking that the amount of "fill" inside the ring obtained with H_2^+ is much larger than that for HeH^+ projectiles. (The space between the ring and the central peak in Fig. 10 is almost empty in the case of HeH^+.)

IV. ANALYSIS AND DISCUSSION

A. Laboratory to center-of-mass transformation

An understanding of the transformation from the laboratory (LAB) frame to the rest frame of the projectile (hereafter referred to as the c.m. frame) is of crucial importance in interpreting the results of these experiments. In the LAB frame a typical measurement consists of determining the yield of a dissociation fragment as a function both of its angular shift (θ_x or, equivalently, θ_y) from the direction of the incident beam (z direction) and of its energy shift (ΔE) from the value $E = \frac{1}{2} m_f V_0^2$ corresponding to the fragment's share of the projectile's kinetic energy (m_f is the fragment's mass, and $\vec{V}_0$ is the beam velocity).

Figure 11 illustrates how these LAB variables are related to the asymptotic c.m. velocity $\vec{v}$ acquired by a fragment following the dissociation of a projectile. Since the momentum transfer is very small in most of the collisions leading to dissociation at these incident energies, we assume here that the projectile c.m. is undeflected in the collisions. If $\vec{V} = \vec{V}_0 + \vec{v}$ is the asymptotic LAB velocity of the fragment, then, for $v \ll V_0$,

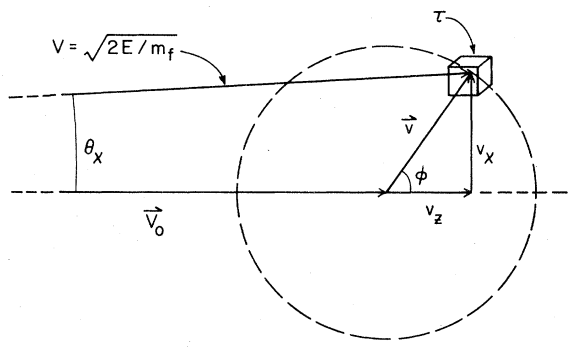

FIG. 11. Kinematical relationships between the parameters (E, θ) measured for the outgoing molecular-ion fragment of mass m_f and its velocity $\vec{v}$ in the center of mass (c.m.) system moving along with the incident ion.

$$\theta_x = v_x/V_0, \quad \theta_y = v_y/V_0, \tag{3a}$$

$$\Delta E = \tfrac{1}{2} m_f (V^2 - V_0^2) \approx m_f v_z V_0, \tag{3b}$$

and

$$\Delta E/E = 2v_z/V_0. \tag{3c}$$

The approximation in Eq. (3b) amounts to ignoring terms with relative magnitude $\sim v/V_0$ (typically, $v/V_0 \approx 5 \times 10^{-3}$ for the cases considered here).

The (LAB) volume element in (θ_x, θ_y, $\Delta E/E$) space is then

$$\tau = \delta\theta_x \delta\theta_y \delta(\Delta E/E) = 2V_0^{-3} \delta v_x \delta v_y \delta v_z. \tag{4}$$

That is, this LAB volume element is directly proportional to the volume element in c.m. velocity space. This simple and convenient relationship is a consequence of the small magnitude of v/V_0; the vector $\vec{V}$ is almost parallel to $\vec{V}_0$ (see Fig. 11), and so the transformation between LAB and c.m. frames, which in velocity space is a simple displacement of the origin by V_0, also amounts (to a good approximation) to a linear transformation between the LAB (θ_x, θ_y, $\Delta E/E$) frame and the c.m. velocity frame.

In the limit, our ability to resolve small differences between fragment velocities in the c.m. is governed by the experimental angular and energy resolutions

$$\delta\theta_x = \delta\theta_y = 3 \times 10^{-4} \tag{5a}$$

and

$$\delta(\Delta E/E) = \delta E/E = 6 \times 10^{-4}. \tag{5b}$$

Combining Eqs. (3) and (5), it can be seen that the three c.m. velocity components are all measured with the same (FWHM) accuracy:

$$\delta v_x = \delta v_y = \delta v_z = 3 \times 10^{-4} V_0. \tag{6}$$

B. Central peaks

Central peaks are observed as dominant features in the ring patterns recorded for gas targets. Although very much less pronounced, central peaks are also observed for H_2^+ and HeH^+ dissociating in the thinnest (~100 Å) foil targets; these peaks disappear rapidly as the foil thickness is increased.

The presence of a central peak implies the production of fragments whose c.m. velocities are near zero. If all of the c.m. velocity components for a given fragment are less than half the value determined by Eq. (6), then that fragment will not suffer a shift in angle or in energy that is detectable within the resolution of our apparatus. [The factor of $\frac{1}{2}$ arises because Eq. (6) gives the FWHM.] For projectile velocities corresponding to 600 keV per nucleon, these considerations indicate that any fragment produced with less than 0.014 eV in the

c.m. frame will be counted in our apparatus as unshifted in angle and energy (i.e., will contribute to the central peak), regardless of the orientation of the incident projectile. Although relatively few dissociations can be expected to produce fragments with c.m. energies as low as this, when such fragments do arise they contribute to the central peak for all projectile orientations. This results in the central peak being greatly enhanced in the observed ring patterns.

In our data the central peaks occur with widths between one and two times the experimental resolution. They therefore correspond to fragments whose asymptotic c.m. kinetic energies are less than about 0.05 eV. For initially stationary bare nuclei, these low energies would imply starting internuclear separations well in excess of 100 Å. Clearly then, in order to account for the existence of fragments with such low c.m. energies, and with the assumption of physically reasonable initial internuclear separations, the effects of electronic screening must be considered. Those dissociations that result in charged fragments being produced a few angstrom apart are unlikely to contribute to the central peak. The central peak must arise predominantly from those dissociation modes that result in the production of one neutral fragment and one charged fragment; hence, we must consider electronic excitation. As one readily infers from an examination of the potential curves shown in Fig. 12, the central peak must receive its main contributions from those dissociations of electronically excited molecular states in which the initial internuclear separations are relatively large (i.e., for the states shown in Fig. 12 greater than, say, about 2.5 Å in H_2^+ and about 1.5 Å in HeH^+). We note too that in considering dissociations liberating c.m. energies on the order of 0.1 eV or less, it is obviously no longer valid to ignore the initial momenta that the fragments have, owing to molecular vibrations and rotations.

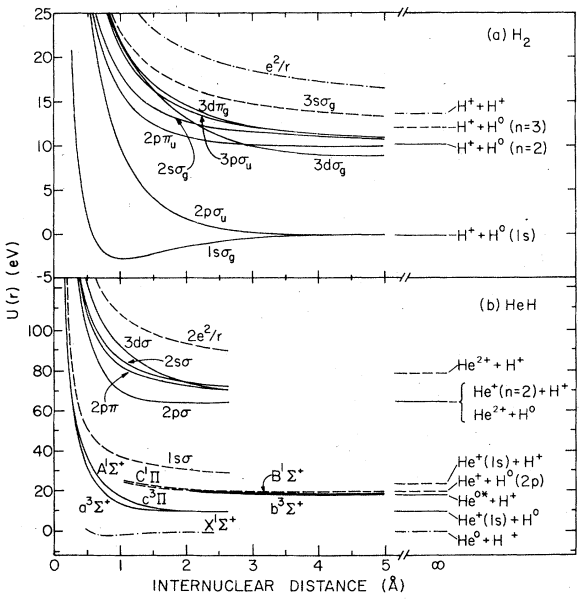

FIG. 12. Interaction potentials for various low-lying electronic states of H_2, H_2^+, HeH^+, and HeH^{2+}.

In their studies of the collisional dissociation of H_2^+ beams at 10 and 50–150 keV in various gases, Valckx and Verveer,[19] and Caudano and Delfosse[20] have observed pronounced central peaks which they attribute to vibrational excitation of the projectiles into low-lying continuum states with energies barely in excess of the asymptotic energy for the $1s\sigma_g$ and $2p\sigma_u$ states of H_2^+. We do not believe this mechanism to be responsible for the central peaks that we observe, first because the relative probability of vibrational excitation is expected[2] to be very small (~1%) and second because our resolution restricts the required c.m. dissociation energies into such a narrow range (< 0.1 eV). In this respect we find our view in accord with that expressed by Gibson and Los,[21] who also observed a strong central peak in their work on the dissociation of 10-keV H_2^+ in gases and explained it as arising from electronic excitation of those H_2^+ ions having large internuclear separations at the moment of impact.

It is interesting to note that while our central peaks have widths about equal to those expected from our experimental resolution, similarly high-resolution work at bombarding energies of about 10 keV (see Ref. 4 for a review) finds central peaks with widths many times the resolution width. The low-energy work also finds fine structure in the neighborhood of the central peak. These differences between observations made at about 10 keV and ours made at a few MeV can primarily be attributed to the fact that the low-energy experiments are sensitive to the detection of incident molecular ions undergoing unimolecular rotational predissociation during their relatively long (~1 μsec) dwell time in the target-gas cell, whereas our dwell times are more than a factor of 10 shorter. The rotationally predissociative states observed and accounted for[4,22-25] in the low-energy work have lifetimes ~1 μsec, i.e., comparable with the flight time to the target and with the dwell time in the target. Our short dwell time makes it improbable that we will observe states with lifetimes ~1 μsec. Furthermore, shorter lifetime states will not survive to reach our target (our flight time from ion source to target is estimated to be ~1 μsec).

We believe that the small central peak observed in our foil data arises from incident projectiles having large internuclear separations. Inside the target the binding electrons are stripped off, but the Coulomb explosion develops only weakly, if at all, during passage through the foil because of the effects of inertia and of screening due to the electrons in the solid. After exiting from the foil the fragments mostly remain stripped and the full Coulomb explosion develops. There is, however, a small chance of electron capture by one of the fragments at the exit surface of the foil. This then precludes a Coulomb explosion, and the charged fragment thus contributes to the central peak observed in the ring pattern. This explanation is consistent with the observed[8,11,16] increase of the relative intensity in the central peak as one goes to thinner foils (less Coulomb explosion inside the foil) and to lower energies (decreased screening lengths inside the foil and increased electron-capture cross sections for the fragments leaving the foil).

C. Reflection method

We discuss now the manner in which we relate our experimentally observed distributions (rings and crosses) to the distribution of initial internuclear separations $D(r)$ and to the molecular potentials $U(r)$ that govern the various dissociation modes. The main part of the procedure we use is sometimes referred to as the reflection method (see, for example, Ref. 1).

We assume that in a dissociative collision the molecular projectile makes a sudden electronic rearrangement while leaving its nuclear constituents unperturbed. That is, we consider the projectile as undergoing a sudden vertical transition (see Fig. 12) up to some excited electronic state which then dissociates, liberating a total c.m. kinetic energy of $U(r)-U(\infty)$, where $U(r)$ is the potential energy at an internuclear separation r for the particular electronic state involved. The relation

$$v=(1/m_f)\{2\mu[U(r)-U(\infty)]\}^{1/2}, \tag{7}$$

where μ is the reduced mass of the projectile, then serves as a mapping function relating the c.m. velocity of a fragment to the potential and to the initial internuclear separation. Figure 13 shows plots of some of the curves for the dissociation energies $U(r)-U(\infty)$.

If we now further assume that the cross section for the electronic excitation is independent of the spatial orientation of the projectile and also independent of its internuclear spacing, then we can readily derive the relationship between the distribution functions for v and r.

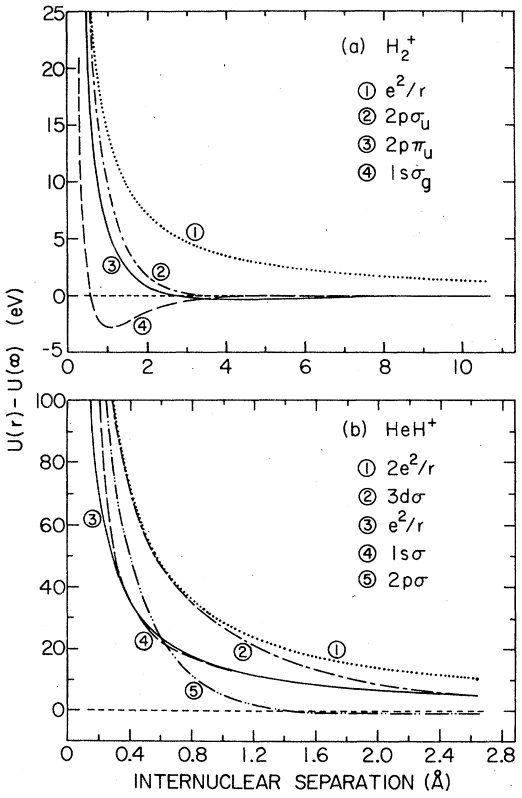

FIG. 13. Interaction potentials used in fitting the c.m. velocity distributions of H^+ from (a) H_2^+ and (b) HeH^+.

$$G(v)=(4\pi v^2)^{-1}D(r)\frac{dr}{dv}, \tag{8}$$

where v and r are related via Eq. (7), and the distribution functions are normalized by

$$\int_0^\infty D(r)\,dr=1 \tag{9}$$

and

$$4\pi\int_0^\infty G(v)v^2\,dv=1. \tag{10}$$

The above assumptions are expected to be more valid for the higher excitations which involve energy transfers much larger than the electronic kinetic energy in the ground state. The validity of these assumptions is discussed in terms of our data in Sec. IV E.

Another way of viewing Eq. (8) is simply to note that for fragments whose c.m. velocities are greater than the limits imposed by our resolution [Eq. (6)], the contribution of a given r value to our measured distributions is spread out over the phase space $4\pi v^2dv$. It is this $1/v^2$ weighting of the measured distributions that required the unweighting procedure described in Eq. (1) of Sec. III.

The reflection method is expected to be valid only for strictly monotonic potentials where $U(r) > U(\infty)$ and therefore fails for values of r corresponding to a potential minimum. This limitation is taken into account in our fitting procedures described in the next sections. For a detailed discussion of the validity and limitations of the reflection method, see Ref. 3.

D. Distribution of initial internuclear separations

Previous studies[7,8,11] of the foil-induced dissociation of MeV beams of H_2^+ and HeH^+ have demonstrated that the observed ring patterns can be quantitatively well understood if one assumes that the projectile's binding electrons are totally stripped off at the instant of entrance into the foil target. The motion inside the foil is then treated as a Coulomb explosion with perturbing effects due to wake forces and multiple scattering. This suggested to us that our data on foil dissociation could be used to determine $D(r)$, the distribution of internuclear separations in the incident projectiles. The function $D(r)$ so obtained can then be used in the analysis of the gas-target data to find out which excited electronic states are involved.

Calculations[7] on the influence of wake forces have shown that they modify the Coulomb explosion least when the projectile's internuclear vector is perpendicular to the beam direction. For instance, for 3-MeV H_2^+ incident upon a 160-Å carbon foil these calculations show that the spacings and peak widths in the angular part of a "cross" are modified by less than 0.5% by wake forces. In the remainder of this section, we therefore restrict our discussion to the angular part of the crosses and we neglect wake effects.

In order to extract a $D(r)$ distribution from an angular distribution one needs to deconvolute the

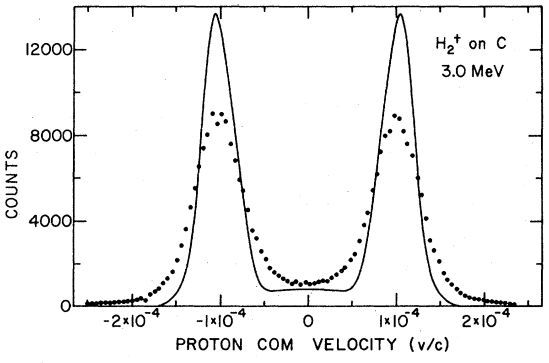

FIG. 14. Distribution function for outgoing H^+ from the dissociation of 3.0-MeV H_2^+ in a 172-Å-thick carbon foil. The points are the data, transformed to c.m. velocity from LAB angular distribution at zero energy shift. The solid curve results from the deconvolution of multiple scattering from these data, as discussed in the Appendix.

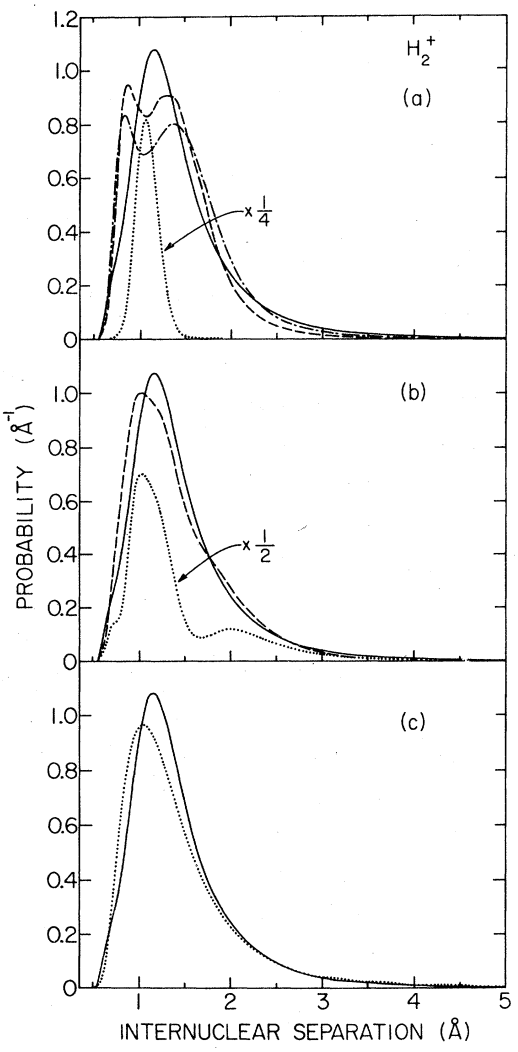

FIG. 15. Radial distribution functions for incident 3.0-MeV H_2^+ ions. The solid curve in (a), (b), and (c) is obtained from the deconvoluted angular distribution given in Fig. 14. In (a), the dashed curve is the radial distribution based on the vibration state distribution derived by von Busch and Dunn (Ref. 26) from the ionization of the ground-vibrational state of H_2; the chained curve is a similar result based on Itikawa's calculations (Ref. 27); the dotted curve is the distribution for the ground-vibrational state of H_2^+ only. In (b), the dotted curve is the radial distribution resulting from ionization of the first excited-vibrational state in H_2, as calculated by von Busch and Dunn, while the dashed curve represents a best fit to our data using a linear combination of the distributions originating from the two lowest-lying vibrational states in H_2. The dotted curve in (c) is a best fit to our data using a linear combination of all 19 vibrational states of the ground-electronic state of H_2^+.

non-negligible effects of multiple scattering and (to a lesser extent) of the experimental angular resolution. The deconvolution procedure that we have used for this is described in the Appendix. Figure 14 shows the result of this unfolding procedure for the case of a H_2^+ beam. [The abscissa in Fig. 14 has been converted from an angle scale to a c.m. velocity scale by means of Eq. (3a).] Because the functional form used for the multiple-scattering distribution has a long tail, there is a region corresponding to high c.m. velocities (near the extreme wings of the data) where the deconvolution is not valid. This translates into a cutoff at small internuclear separations (at about $r = 0.5$ Å) in the derived distribution $D(r)$.

In this manner, and using a pure Coulomb potential in Eq. (7), we have derived the distributions shown in Figs. 15 and 16 for $D(r)$ in H_2^+ and HeH^+, respectively. Also shown in each figure is the calculated distribution for the vibrational and electronic ground state. For H_2^+, where it was thought to be reasonable to assume that the molecular ion is formed by direct ionization of H_2, we show additional distributions $D(r)$ calculated on the basis of H_2^+ vibrational populations given by (i) the (approximate) Franck-Condon factors of von Busch and Dunn,[26] (ii) the parameters of Itikawa[27] (these are parameters used in a computation that gives excellent agreement with the observed[28] photoelectron intensities from H_2), and (iii) a mixture of H_2^+ level populations obtained, assuming the initial H_2 to be 58% in the ground state and 42% in the first excited vibrational state, using Itikawa's and von Busch and Dunn's population parameters, respectively.

The derived distributions $D(r)$ show the most probable values of r to be 1.17 Å for H_2^+ and 0.80 Å for HeH^+. These may be compared with values of 1.08 and 0.79 Å obtained for the ground states alone in H_2^+ and HeH^+, respectively. For HeH^+ the derived $D(r)$ is about 1.5 times wider than expected from the ground state alone. This fact, together with the small overall shift of the distribution towards higher r values, indicates that most of the HeH^+ ions are incident in the ground vibrational state with a relatively small fraction in the first one or two vibrationally excited states. Specifically, we find that the four lowest-lying vibrational states of HeH^+ represent 53%, 22%, 11%, and 6%, respectively, of the incident beam. For H_2^+, on the other hand, excited vibrational levels are clearly much more involved, although the population of these higher vibrational levels is significantly less than has been assumed by other authors[29-31] in analyzing Coulomb explosion experiments. Table III presents the distribution of incident vibrational states derived from our data and compares our results with those of von Busch and Dunn,[26] which are typical of those assumed by pre-

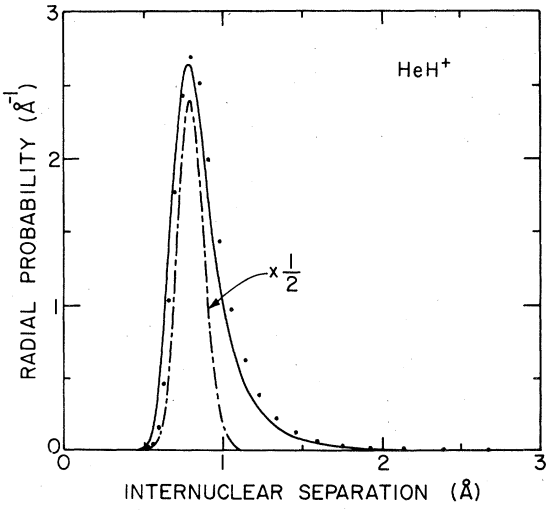

FIG. 16. Radial distribution function for incident 3.63-MeV HeH^+ ions. The points are derived from the data. The solid curve is the best fit to the data, obtained by adjusting the fractional contribution of each of the nine vibrational levels of the electronic ground state. The chained curve is the distribution for the ground-vibrational state only.

TABLE III. Distribution of vibrational levels of H_2^+, expressed as a percentage of the total incident beam, obtained from fitting our measured radial distribution (the solid curves in Fig. 15). For comparison, a distribution (Ref. 26) representative of those assumed by other authors (Refs. 29–31) is also given.

v	This work	Reference 26
0	19.2	11.7
1	15.5	18.7
2	12.1	18.6
3	9.7	15.0
4	7.7	12.3
5	6.3	7.4
6	5.1	5.1
7	4.2	3.7
8	3.4	2.4
9	2.9	1.6
10	2.2	1.2
11	1.8	0.81
12	1.4	0.56
13	1.5	0.37
14	1.2	0.25
15	1.1	0.17
16	0.41	0.11
17	0.21	0.06
18	4.3	0.01

vious authors.

We believe that the factors most likely responsible for the deviation of our derived $D(r)$ for H_2^+ from a Franck-Condon-like distribution[26] are first the fact that in the ion source the initial H_2 is not always in its ground state and second the fact that the higher vibrational states of H_2^+ are depleted either in the high-pressure ion-source region or in the accelerator and flight tube en route to the target. In the ion source, the high vibrational states may be preferentially collisionally deexcited, and en route to the target the now swift ions may have their high vibrational states preferentially dissociated by collisions with residual gas in the vacuum system. We have noted that the results we obtain are not observably dependent upon the ion-source parameters that are presently at our disposal to vary. In addition, autoionization of high Rydberg states and rotational effects may play a role in the ion source.[26]

Attempts to fit vibrational state populations to our measured radial distributions [Figs. 15(c) and 16] are only moderately successful. It is worth noting that our derived distributions can be expected to be in error for internuclear separations that are large compared with the characteristic electronic screening distance for fast ions traversing carbon. Assuming this distance to be $a = V_0/\omega_p$, where ω_p is the volume plasma frequency of carbon, we obtain $a = 4.3$ and 3.0 Å for 3.0-MeV H_2^+ and 3.63-MeV HeH^+, respectively. We have not made any correction for screening effects in our derivation of $D(r)$ (such effects would produce a very slight shift to a lower r). A possible explanation for our failure to obtain a better fit to a vibrational population may be the presence in the incident beam of bound H_2^+ molecules in higher electronic states. This would produce a shift toward somewhat larger internuclear separations.

E. Analysis of results for gas targets

Using the distributions $D(r)$ derived from the foil data, we have made similar analyses of the gas data, postulating as dissociative potentials the various $U(r)$ shown in Fig. 12. For these data, no effects due to wake forces or multiple scattering needed to be taken into account.

It was found that no single excited electronic state is adequate to fit the observed velocity distributions. Thus, for example, states such as the $2p\pi_u$ in H_2^+ give a fair description of the low-velocity part of the spectrum, but the high-velocity part cannot be described without the inclusion of a Coulomb contribution. In our analysis velocity distributions were first calculated for each of the potentials shown in Fig. 12. These were then combined with weighting factors to obtain the best fits to the data. The results of this fitting procedure are shown in Figs. 17 and 18. Because of the limitations of the reflection method in the tail regions of the potentials (discussed in Sec. IV C), the fitting was performed only for $v/c > 0.5\times10^{-4}$. The same procedure was followed for both the longitudinal velocity spectra (energy scans) and the transverse velocity spectra (angular scans) and yielded similar results.

For H_2^+ the best fit was obtained with a combination of the $2p\pi_u$ (10%) and the Coulomb (90%) states. The $2p\sigma_u$ contribution was found, within fitting errors, to be zero for both orientations of the projectile. The potential functions used in the H_2^+ fit were taken from the tabulation of Sharp.[32] For keV bombarding energies, the $2p\sigma_u$ state plays a dominant role, and it is somewhat surprising that it makes no contribution in our experiments. There is evidently a favoring of the more highly excited states (including ionization) at the higher energies involved in our work. It may also be that the $2p\sigma_u$ is artificially suppressed in our analysis because of our underlying assumption that the ex-

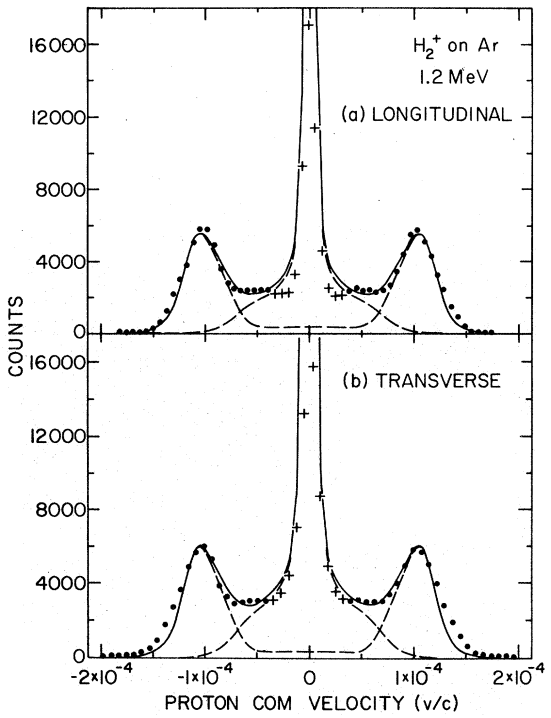

FIG. 17. Measured c.m. velocity distributions and least-squares fits for outgoing H^+ from 1.2-MeV H_2^+ incident on Ar gas at a pressure of 9.8 mTorr. Only data points shown as solid circles, corresponding to $(v/c) \geq 5\times10^{-4}$, were fitted.

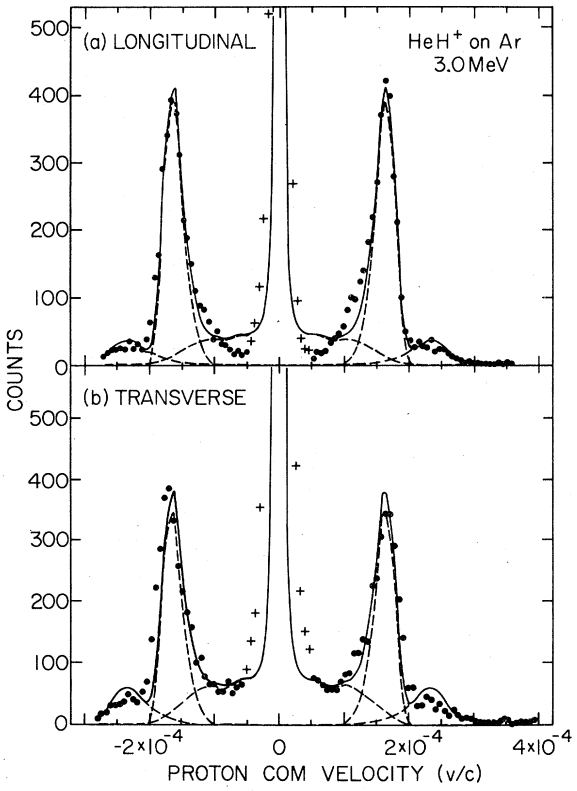

FIG. 18. Measured c.m. velocity distributions and least-squares fits for outgoing H^+ from 3.0-MeV HeH^+ incident on Ar gas at a pressure of 16.4 mTorr. Only data points shown as solid circles, corresponding to $(v/c) \geq 5\times10^{-4}$, were fitted.

citation cross section is independent of r. This assumption is expected to be less valid for the $2p\sigma_u$ than for higher states. Peek[33] has shown that for high projectile energies the $2p\sigma_u$ excitation probability increases with increasing r, thereby emphasizing the low-velocity region where our reflection-method calculation is least valid. Thus our c.m. velocity distribution calculated for the $2p\sigma_u$ state would be rejected in the fit because of the overly emphasized high-velocity region. In addition, the very large impact parameters needed for such gentle excitations at these beam energies (~4 Å for $2p\sigma_u$ excitation on Ar at 1.2 MeV) greatly exceed the dimensions of atomic screening radii. One might therefore expect that there should be a preference for higher excitations.

Analysis of the HeH^+ distributions is more complicated because there are more final states to be considered for this two-electron system. The lowest-lying excited electronic states of HeH^+ that dissociate asymptotically into a proton and a neutral helium atom are the $b^3\Sigma^+$ and $B^1\Sigma^+$ states. These are therefore the most natural states to try for a fit to the low-velocity region of the proton spectra from HeH^+. However, the deep (several eV) minima of these curves preclude calculations with the reflection method. Hence, these potentials were rejected in the fitting procedure. The best fit to the data was obtained with only three electronic states of the HeH^{2+} system (the $1s\sigma$, $2p\sigma$, and $3d\sigma$ united atoms designations). The $1s\sigma$ and $3d\sigma$ states are repulsive and, at small separations, quite similar to the pure Coulomb potentials of $He^+ + H^+$ and $He^{2+} + H^+$, respectively. They are, however, screened potentials and do not vary as $1/R$ at larger distances (see Fig. 13). The $2p\sigma$ state is partially attractive, having a slight potential minimum at ~2-Å separation. This attraction is caused by the polarization of the H(1s) by the field of the He^{2+} dissociation partner. The potential functions for HeH^+ were taken from the work of Michels,[34] and Kolos and Peek,[35] and for the HeH^{2+} from the work of Bates and Carson.[36] Similar fits were obtained for the He^+ and He^{2+} spectra, as well as for the protons.

The fits in Fig. 18 were relatively unaffected by our choice of the $3d\sigma$ and $1s\sigma$ over bare Coulomb potentials, since the contribution to the central peak is minimal for each. The fits show that the dissociation is dominated by the $He^+(1s) + H^+$ dissociation channel (the $1s\sigma$ electronic state of the united HeH^{2+}), in agreement with the observation of Stearns *et al.*[17] For the longitudinal (E) orientation, we find 68%, 10%, and 23% contributions for dissociation through the $1s\sigma$, $2p\sigma$, and $3d\sigma$ channels, respectively. The transverse (θ) orientation gives 54%, 14%, and 32%, demonstrating the weak orientation dependence of the excitation cross sections. As the uncertainties associated with fitting the individual spectra are at most a few percent, the stated variation in these fractional components from one orientation to the other is representative of the overall uncertainty in the relative contributions of the various dissociation channels.

The fits, though not as good as in the H_2^+ case, do demonstrate the qualitative features of the HeH^+ dissociation. As in the case of H_2^+, there is a preference for higher excitation and ionization over more gentle collisions. Our neglect of the two-electron system, as well as several other electronic states of HeH^{2+}, could account for our failure to explain the wide central peaks and detailed structures that are observed in the data.

An alternative approach to these data is simply to use an exponentially screened Coulomb potential of the form

$$U(r) = (Z_1 Z_2)_{\text{eff}}(e^2/r)\exp(-r/a) \qquad (11)$$

to represent the interaction between the two frag-

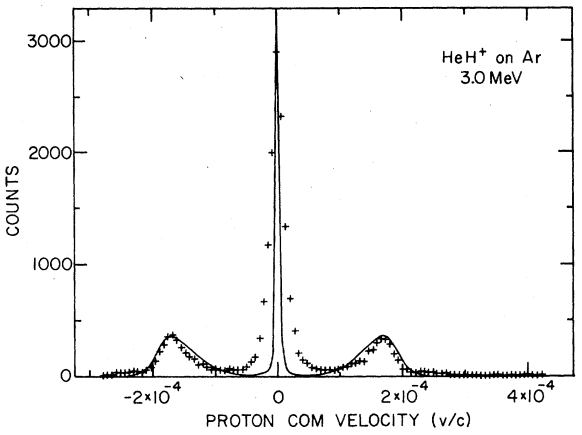

FIG. 19. Same data as in Fig. 18 (b), fitted with an angular distribution calculated using a screened Coulomb potential whose parameters were adjusted to fit the ratio of central peak to outer peak intensity. Additional details are discussed in the text.

ments, where a is a screening parameter to be determined and $(Z_1Z_2)_{eff}$ is a product effective charge. While such a simple parametrization clearly cannot duplicate the detailed structure observed in spectra such as in Figs. 17 and 18, it does help illustrate the important role of electronic screening in the occurrence of central peaks in the data for solid targets. Such calculations do give qualitative agreement with the data (see Fig. 19) with physically reasonable values for $(Z_1Z_2)_{eff}$ and a. For the 3-MeV-HeH$^+$ gas data with $(Z_1Z_2)_{eff} = 1.8$ and $a = 1.5$ Å, the relative intensities of central and outer peaks are well reproduced.

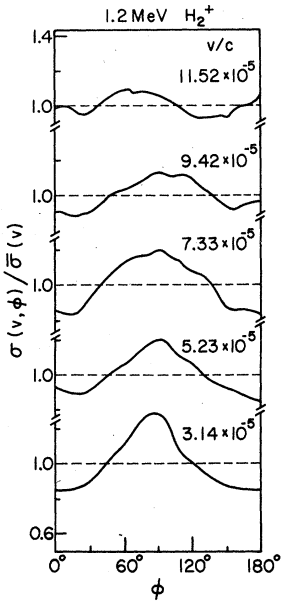

FIG. 20. Center-of-mass angular distributions for outgoing H$^+$ having various c.m. velocities. These curves are derived from the data presented in Fig. 9 for 1.2-MeV H_2^+ dissociating in 7.8-mTorr Ar.

Finally, in this section we point to some aspects of our data indicating that the cross sections for electronic excitation do indeed display an orientation dependence, especially for large internuclear separations. This is illustrated for the case of H_2^+ in Fig. 20, where we show the relative yields of protons as a function of the angular coordinate on circular paths prescribed about the central peak of the ring pattern of Fig. 9. Varying the position on one of these circular paths is equivalent to altering the polar angle (ϕ in Fig. 11) between the internuclear vector and the beam direction for a fixed c.m. velocity v. One sees that for large v (where the excitation is primarily to the fully ionized state) the excitation probability is essentially independent of orientation. But for small v (excitation mainly to the $2p\pi_u$ state) the excitation probability is strongly peaked at 90° (transverse orientation). This behavior is in harmony with predictions based on the calculations of Peek[33] and the observations in several experiments at bombarding energy[4] ~ 10 keV, although both the calculations and the experiments at low energies deal predominantly with the $2p\sigma_u$ state in H_2^+. Similar behavior is seen in our data on HeH$^+$, as is evident from a cursory glance at Figs. 10 and 18.

V. IMPLICATIONS

The existence of a strong central peak in the c.m. velocity distribution of fragments from the collision-induced dissociation of molecular ions in gases offers some insight into a number of phenomena associated with the passage of molecular ions through solid targets. These include the existence of central peaks in the velocity distribution of dissociation fragments emerging from thin foil targets, the transmission of molecular ions through thin foils,[8,37] and the observed velocity distribution of neutral dissociation fragments.[8,15]

A. Central peaks seen with foil targets

Though not as prominent a feature of the c.m. velocity spectra of dissociation fragments for solid targets as for gas targets, central peaks have been observed with foil targets for outgoing H$^+$ from incident H_2^+ and HeH$^+$ (see Figs. 3 and 4) and for outgoing $^3He^{++}$ from incident $^3He_2^+$ (see Ref. 8). (There was, however, no central peak in the case of outgoing $^3He^+$ from incident $^3He_2^+$ under identical circumstances.) Fragments which fall within such a central peak must have experienced a very gentle Coulomb explosion while moving through the solid foil, followed by the neutralization of at least one of the emerging fragments on

leaving the foil target.

The importance of electron capture for neutralizing one of the outgoing fragments is well illustrated by the dissociation of $^3He_2^+$. With a decreased probability for capturing a sufficient number of electrons at the rear surface of the target, the magnitude of the central peak should be decreased. This explains the absence of the central peak for outgoing $^3He^+$, though it is present for outgoing $^3He^{2+}$ (for incident $^3He_2^+$ on a thin carbon foil in each case). In the former case only two electrons need be captured during the brief transition from the foil to the vacuum behind it, while three electrons are required to produce $^3He^0 + {}^3He^+$ as the two fragments.

In addition to requiring electron capture at the exit, the presence of a central peak in the foil measurements demonstrates that there is a finite probability that a molecular cluster can traverse a foil and impart only a negligible kinetic energy to its fragments. For a given incident velocity one expects this probability to be larger for thinner targets, where the repulsive forces between the fragments act for a shorter time. This is borne out by our data, which exhibit central peaks only for the thinnest of carbon foils.

Furthermore, only those incident molecular ions contribute to the central peak which have an initial internuclear separation larger than some critical value. In the case of gas targets, this critical separation was the effective range of the repulsive force between the two dissociating fragments, at least one of which was neutral. In the solid, both fragments are charged as they move through the foil and each experiences a relatively large Coulomb repulsion. However, this repulsive force acts only while the fragments are inside the foil and is abruptly turned off if one of the fragments is neutralized at the rear surface of the foil. Thus it is the effective charge and the mass of the two ions and their dwell time inside the foil which determine this critical initial separation for solid targets. For example, for 1.2-MeV H_2^+ incident on a 100-Å foil, all incident ions with an incident internuclear separation greater than 2 Å will produce protons having less than 0.053-eV c.m. kinetic energy at the rear side of the target.

B. Molecular ion transmission

The existence of central peaks in gas target data and in solid target data offers some insights into the mechanisms by which molecular ions can traverse thin solid foils and emerge intact, as has recently been reported for a range of molecular ions and targets.[8,37] Figure 21 presents some representative data for the fraction of HeH^+ ions transmitted through carbon foils.

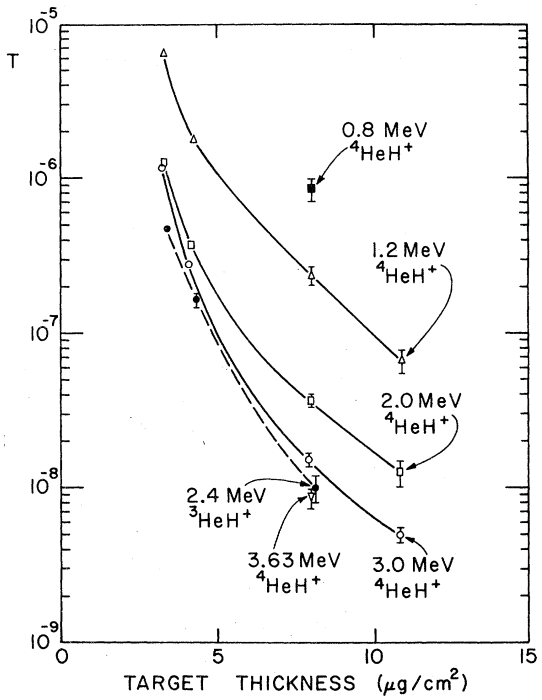

FIG. 21. Measured fraction T of HeH^+ ions transmitted through carbon foils of various thicknesses.

The crux of the problem, in accounting for these data, is to explain how the constituents of the incident ion can be stripped of their outer electrons on entering the foil, undergo a Coulomb explosion while traversing the foil, capture an appropriate number of electrons at the rear surface of the foil, and still have some fraction (10^{-3}–10^{-11}) not continue to dissociate owing to the relatively large separation and excess kinetic energy which they then possess. But these are exactly the issues that were relevant to the observation of central peaks for solid targets. Ions which enter the foil with small internuclear separations will undergo relatively violent Coulomb explosions during their dwell time ($\sim 10^{-15}$ s), inside the foil, converting much of their electrostatic potential energy into kinetic energy in the c.m. system. There are no credible mechanisms for dissipating this kinetic energy quickly enough ($\sim 10^{-15}$ s) after the ion leaves the foil to prevent these ions from dissociating, even if they have captured sufficient electrons on exiting from the foil.

On the other hand, ions which enter the foil with larger internuclear separations (e.g., $r \gtrsim 2$ Å for 1.2-MeV H_2^+) will undergo much less violent Coulomb explosions during the same dwell time in the foil. The existence of incident ions having such large internuclear separations is demonstrated by the large central peaks in our gas data. The non-

zero probability for capturing a sufficient number of electrons at the rear surface of the foil is demonstrated by the observed central peaks in our solid target data. Furthermore, the relatively small amount of kinetic energy released during the Coulomb explosion of these ions will not cause their dissociation, provided it is less than the dissociation energy of the particular attractive state of the molecular ion formed on leaving the foil. These dissociation energies are typically 1–3 eV. In fact, the relatively large internuclear separation and low c.m. kinetic energy of two such fragments when they capture one or more binding electrons at the rear side of the target foil may allow the formation of long-range bound states such as the $2p\pi_u$ and $3d\sigma_g$ states of H_2^+. Such long-range bound states of positive molecular ions have been predicted[38] but never directly observed. Their preferential formation in beams of molecular ions transmitted through solid targets is a possibility we are currently investigating.

From this point of view, the formation of central peaks in the c.m. velocity distribution of outgoing fragments and the transmission of molecular ions through thin foils merely represent two possible outcomes of the same sequence of events, namely, a gentle Coulomb explosion of the two fragments inside the foil followed by an electron capture while leaving the foil. Transmission occurs when the electron capture produces a bound state of the molecular ion; a fragment with a low c.m. kinetic energy results from the formation of a short-range repulsive electronic state of the molecular ion.

Quantitative analysis of such transmission data is beyond the scope of this paper and will be published separately. However, two general features of the data should be noted: (i) For all cases where we observe central peaks in the energy distribution of one of the exploded fragments emerging from a solid target, we find that there is also a high yield for transmission of the molecular ion, and (ii) we do not see transmission in any case in which the incident ion does not contain either H or He as a constituent, which again emphasizes the importance of electron capture at the rear surface of the foil. Higher charged ions must capture a larger number of these electrons to form bound molecular ions, thus greatly reducing the probability of recombination of the ion fragments downstream of the target foils for incident ions such as O_2^+ or CO^+.

C. Neutral fragments

We have also performed measurements on the distribution of neutral fragments arising from dissociations in solid targets. Representative ring distributions for observed H^0 are shown in Fig. 22(a) for 3.0-MeV $H_2^+ \rightarrow H^0$ and Fig. 22(b) for 3.63-MeV $HeH^+ \rightarrow H^0$. There are several striking features seen when comparing these two figures.

The minimum on the high-energy side of the $HeH^+ \rightarrow H^0$ ring is apparently an orientation-dependent electron-capture phenomenon which will be discussed in a future publication. Even more con-

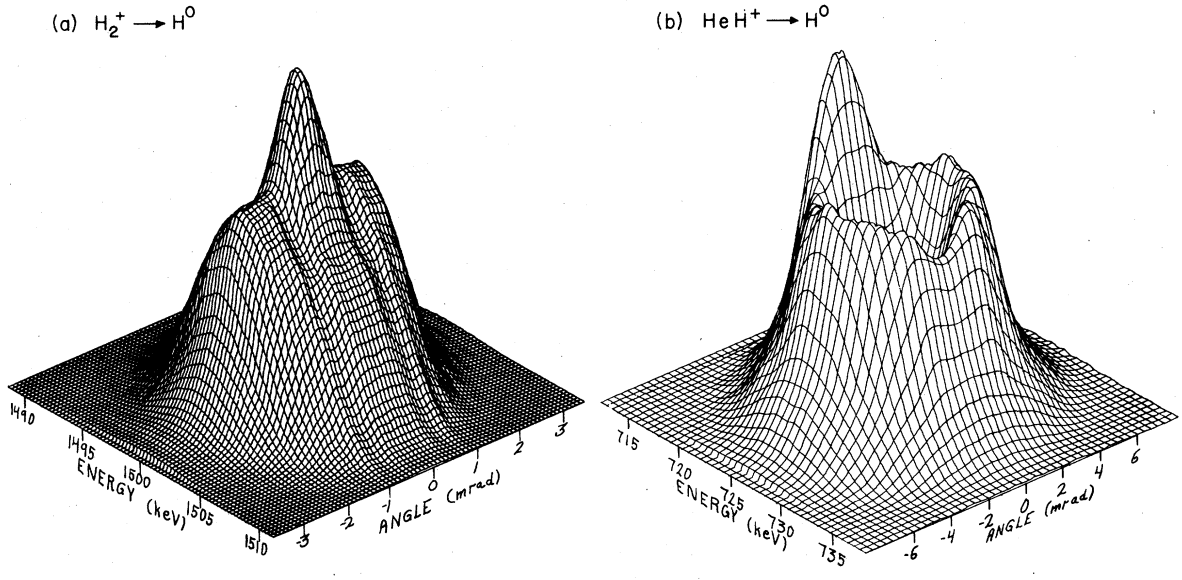

FIG. 22. Ring patterns for (a) 3.0-MeV $H_2^+ \rightarrow H^0$ in a 132-Å carbon foil and (b) 3.63-MeV $HeH^+ \rightarrow H^0$ in a 144-Å carbon foil.

spicuous, however, in the $H_2^+ \rightarrow H^0$ data, is the dominance of the central peak structure over the ring corresponding to the fully exploded fragments. (Similar data have recently been reported by Gaillard *et al.*[15]) The $HeH^+ \rightarrow H^0$ structure does show a very slight central peak, similar to the $HeH^+ \rightarrow H^+$ structure, which cannot be observed in Fig. 22(b). This apparent difference between the H_2^+ and HeH^+ data is not so much a reflection of different phenomena as it is a consequence of the $1/v^2$ scaling of the distributions and the smaller Coulomb energy of H_2^+. When multiplied by v^2, both the H_2^+ and HeH^+ distributions are quite similar to one another and are consistent with the picture of a normal charged explosion in the foil, including wake effects, that is truncated by electron capture at exit. If bound neutral hydrogen atoms exist while the protons move through the solid, as has been recently suggested,[16,39] such neutral atoms represent a very small fraction of the H^0 that are observed outside the foil. By integrating the measured ring patterns in annular sections, we consistently find the flux in the center to represent $\ll 0.1\%$ of the total intensity of these distributions.

D. Tandem accelerators

Finally, we note the important role of excited electronic states in the stripping of heavy molecular ions at the high-voltage terminals of tandem accelerators. For a variety of heavy-ion beams it has been necessary to accelerate negative molecular ions because sufficient intensities of the desired negative monatomic-ion beams are not achievable. When passed through a foil stripper at the terminal, these beams are severely degraded in quality owing to the energy and angle spreads introduced by the Coulomb explosion. As Middleton has pointed out,[40] several groups have found that this problem can be substantially reduced by preceding the foil stripper with a gas stripping stage.

From the foregoing discussion it is now clear why this well-known "folklore" works. As in our H_2^+ and HeH^+ gas experiments, the interaction of the heavy molecular ions with the stripper-gas atoms includes a significant fraction of large impact-parameter collisions which excite the electrons of the molecular ion to repulsive states. Dissociation of these molecular ions produces many fragments of low relative velocity. After these fragments travel a few microns, they are separated by several hundred angstrom. Subsequent stripping in a solid foil yields high charge states without introducing any further energy or angle spread.

E. Summary

We have examined the collision-induced dissociation of MeV molecular-ion beams in gases and have found that the excitation of repulsive electronic states can account for the c.m. velocity spectra of the outgoing charged fragments. The relation of these data to the transmission and fragmentation of molecular ions in foil targets has been discussed. For foil targets all incident ions experience a Coulomb explosion inside the solid. Some fraction of the fragments emerging from the foil captures one of more electrons, forming repulsive or attractive molecular-ion states. Of these, the fragments which had the largest internuclear separations on entering the target foil produce outgoing fragments having low c.m. kinetic energy (for repulsive electronic states) or transmitted molecular ions (for attractive electronic states). A quantitative test of this model is difficult with the present data because central peaks are observed clearly only with the very thinnest targets at short dwell times. Experiments are under way in this laboratory to gather comprehensive data on the energy and target thickness dependences of central peaks by measuring charged-neutral coincidences.

ACKNOWLEDGMENTS

We gratefully acknowledge many helpful conversations with J. E. Monahan and J. Berkowitz. We thank G. E. Thomas for his assistance in supplying the thin carbon foils used in this work. Four of us (P.J.C., K. -O.G., W.J. P., and Z.V.) want to take the opportunity to thank Argonne National Laboratory for its generous support and hospitality during our visits. One of us (K. -O.G.) acknowledges the support of the Gesellschaft für Schwerionenforschung and the Bundesministerium für Forschung und Technologie. This work was performed under the auspices of the U. S. Department of Energy, Division of Basic Energy Sciences.

APPENDIX

The angular distributions of protons from H_2^+ and HeH^+ incident on thin carbon targets are modified by multiple scattering. The problem of reconstructing an unmodified angular distribution, given by the generalized vector $\underline{g}$, from the measured distribution $\underline{c}$ is in principle just the mathematical problem of inverting the matrix equation

$$\underline{c} = K \cdot \underline{g}, \tag{A1}$$

where K is a matrix operator that represents the response function of the measuring system.

In actual practice, the inversion of K is a difficult problem and has been discussed in detail by Monahan.[41] The main difficulty arises from the statistical nature of $\underline{c}$ and K. As a result, small

statistical errors in $\underline{c}$ are amplified by the nearly singular operator K^{-1} so that the solution

$$\underline{g} = K^{-1} \cdot \underline{c} \tag{A2}$$

is often completely meaningless. To circumvent this difficulty, we have used an iterative technique suggested in Ref. 41 to accomplish the unfolding.

We decompose K in the form

$$K = \eta I - B , \tag{A3}$$

where I is the unit matrix and η is a scalar constant. Substituting into Eq. (A1) and rearranging give

$$\underline{g} = (1/\eta)(\underline{c} + B \cdot \underline{g}) . \tag{A4}$$

This equation may be solved iteratively, yielding, on the ith iteration,

$$\underline{g}^{(i)} = (1/\eta)(\underline{c} + B \cdot \underline{g}^{(i-1)}) . \tag{A5}$$

By terminating the iteration process after a few iterations (~ 10 in our case), spurious contributions associated with small eigenvalues are almost completely eliminated. Those contributions begin to appreciably affect the result only after many iterations.

Our response operator K was taken to be a matrix whose $\alpha\beta$ element was given by:

$$K_{\alpha\beta} = \left(\frac{\sigma_n^2}{(\theta_\alpha - \theta_\beta)^2 + \sigma_n^2} \right)^n , \tag{A6}$$

where θ_α is the angle associated with channel α in the fragment angular spectrum. The value of n was selected to give smooth, monotonic tails in each deconvoluted spectrum. For H_2^+, $n = 2$; for HeH^+, $n = 1.4$.

For each value of n used, the value of the width σ_n was adjusted to reproduce the expected FWHM due to the combined effects of multiple scattering and the experimental angular resolution, namely, 1.8×10^{-5} in units of v/c.

Because of the finite range of the data, the deconvolution oscillates at large values of v/c after only a few iterations. We therefore sacrifice our knowledge of the spectrum at large v/c to determine more accurately the low-velocity region. As a result, this procedure produces a cutoff in the derived radial distributions for $r \lesssim 0.5$ Å.

---

*Visiting Scientist at Argonne National Laboratory. Permanent address: Middlebury Coll., Middlebury, Vt. 05753.

†Summer visitor at Argonne National Laboratory. Permanent address: Univ. of Frankfurt, W. Germany.

‡Visiting Scientist at Argonne National Laboratory. Permanent address: Univ. of Cologne, W. Germany.

§Present address: N. Y. State Dept. of Health, Albany, N. Y. 11201.

¶Summer visitor at Argonne National Laboratory. Permanent address: Weizmann Institute of Science, Rehovoth, Israel.

[1] *Collision Spectroscopy*, edited by R. G. Cooks (Plenum, New York, 1978).

[2] E. E. Salpeter, Proc. Phys. Soc. London, Sect. A 63, 1295 (1950).

[3] G. W. McClure and J. M. Peek, *Dissociation in Heavy Particle Collisions*, (Wiley, New York, 1972).

[4] J. Los and T. R. Govers, in *Collision Spectroscopy*, edited by R. G. Cooks (Plenum, New York, 1978), Chap. 6.

[5] N. Bohr, K. Dan. Vidensk. Selsk. Mat. -Fys. Medd. 18, 1 (1948).

[6] D. S. Gemmell, J. Remillieux, J. -C. Poizat, M. J. Gaillard, R. E. Holland, and Z. Vager, Phys. Rev. Lett. 34, 1420 (1975).

[7] Z. Vager and D. S. Gemmell, Phys. Rev. Lett. 37, 1352 (1976).

[8] D. S. Gemmell, P. J. Cooney, W. J. Pietsch, A. J. Ratkowski, Z. Vager, B. J. Zabransky, A. Faibis, G. Goldring, and I. Levine, in Proceedings of the 7th International Conference on Atomic Collisions in Solids, 1977 (unpublished).

[9] A. Faibis, G. Goldring, and Z. Vager, Phys. Rev. Lett. 39, 695 (1977).

[10] D. S. Gemmell, E. P. Kanter, and W. J. Pietsch, Chem. Phys. Lett. 55, 331 (1978).

[11] Z. Vager, D. S. Gemmell, and B. J. Zabransky, Phys. Rev. A 14, 638 (1976).

[12] D. S. Gemmell, Z. Vager, and B. J. Zabransky, in *Proceedings of the 4th Conference on Scientific and Industrial Applications of Small Accelerators, Denton, Tex.*, 1976 (IEEE, New York), p. 329.

[13] J. Golovchenko and E. Laegsgaard, Phys. Rev. A 9, 1215 (1974).

[14] D. S. Gemmell, J. Remillieux, J. -C. Poizat, M. J. Gaillard, R. E. Holland, and Z. Vager, Nucl. Instrum. Methods 132, 61 (1976).

[15] M. J. Gaillard, J. -C. Poizat, and J. Remillieux, Phys. Rev. Lett. 41, 159 (1978).

[16] R. Laubert and F. K. Chen, Phys. Rev. Lett. 40, 174 (1978).

[17] J. W. Stearns, K. H. Berkner, R. V. Pyle, B. P. Briegleb, and M. L. Warren, Phys. Rev. A 4, 1960 (1971).

[18] K. H. Berkner, S. N. Kaplan, R. V. Pyle, and J. W. Stearns, Phys. Rev. 146, 9 (1966).

[19] F. P. G. Valckx and P. Verveer, J. Phys. (Paris) 27, 480 (1966).

[20] R. Caudano and J. M. Delfosse, J. Phys. B 1, 813 (1968).

[21] D. K. Gibson and J. Los, Physica (Utrecht) 35, 258 (1967).

[22] J. Schopman and J. Los, Physica (Utrecht) 48, 190 (1970).

[23] J. M. Peek, Physica (Utrecht) 64, 93 (1973).

[24] J. G. Maas, N. P. F. B. Van Asselt, and J. Los, Chem.

Phys. 8, 37 (1975).
[25]P. G. Fournier, G. Comtet, R. W. Odom, R. Locht, J. G. Maas, N. P. F. B. Van Asselt, and J. Los, Chem. Phys. Lett. 40, 170 (1976).
[26]See, for example, F. von Busch and G. H. Dunn, Phys. Rev. A 5, 1726 (1972).
[27]Y. Itikawa, J. Electron Spectrosc. Relat. Phenom. 2, 125 (1973).
[28]J. Berkowitz and R. Spohr, J. Electron Spectrosc. Relat. Phenom. 2, 143 (1973).
[29]J. Remillieux, in *Proceedings of the Fifth International Congress of Radiation Research* (Academic, New York, 1975), p. 302.
[30]J. W. Butler and C. M. Davisson, Nucl. Instrum. Methods 149, 183 (1978).
[31]D. Nir, A. Weinberg, A. Mann, M. Meron, and S. Gordon, Phys. Rev. A 18, 1399 (1978).
[32]T. E. Sharp, At. Data 2, 119 (1971).
[33]J. M. Peek, Phys. Rev. 134, A877 (1964).
[34]H. H. Michels, J. Chem. Phys. 44, 3834 (1966).
[35]W. Kolos and J. M. Peek, Chem. Phys. 12, 381 (1976).
[36]D. R. Bates and T. R. Carson, Proc. R. Soc. London Ser. A 234, 207 (1956).
[37]J. -C. Poizat and J. Remillieux, Phys. Lett. A 34, 53 (1971).
[38]G. H. Dunn, R. Geballe, and D. Pretzer, Phys. Rev. 128, 2200 (1962).
[39]M. C. Cross, Phys. Rev. B 15, 602 (1977).
[40]R. Middleton, from a talk presented at the SNEAP Conference, Los Alamos, N.M., 1977, LASL report number LA7445C.
[41]J. E. Monahan, in *Scintillation Spectroscopy of Gamma Radiation*, edited by S. M. Shafroth (Gordon and Breach, New York, 1967).